Scanning tunneling spectroscopy on $SrFe_2(As_{1-x}P_x)_2$

Jasmin Jandke,[1] Petra Wild,[1] Michael Schackert,[1] Shigemasa Suga,[2] Tatsuya Kobayashi,[3] Shigeki Miyasaka,[3] Setsuko Tajima,[3] and Wulf Wulfhekel[1]

[1]*Physikalisches Institut, Karlsruher Institut für Technologie, 76131 Karlsruhe, Germany*

[2]*Institute of Scientific and Industrial Research, Osaka University, 8-1 Mihogaoka, Ibaraki, Osaka 567-0047, Japan*

[3]*Department of Physics, Graduate School of Sciences, Osaka University, Osaka 560-0043, Japan*

(Received 17 December 2015; revised manuscript received 3 March 2016; published 28 March 2016)

We investigated $SrFe_2(As_{1-x}P_x)_2$ single crystals with four different phosphorus concentrations x in the superconducting phase ($x = 0.35,0.46$) and in the magnetic phase ($x = 0,0.2$). The superconducting samples display a V-shaped superconducting gap, which suggests nodal superconductivity. Furthermore, we determined the superconducting coherence length by measuring the spatially resolved superconducting density of states. Using inelastic tunneling spectroscopy, we investigated excitations in the samples with four different phosphorus concentrations. Inelastic peaks are related to bosonic modes. The phonon and nonphonon mechanisms for the origin of these peaks are discussed.

DOI: 10.1103/PhysRevB.93.104528

I. INTRODUCTION

Ever since the first iron-based superconductors with LaOFeAs were discovered in 2008 [1], many new iron-based superconductors have been found. In spite of intensive investigations using a variety of techniques, the superconducting pairing mechanism and the microscopic origin of magnetism in iron-based superconductors are still under debate [2]. Nevertheless, combining different results accumulated so far, knowledge about the physical properties of iron pnictides has progressed. With regard to the determination of the pairing mechanism, the key properties are the pairing symmetry and the investigation of bosonic excitations, which probably act as the "pairing-glue" for Cooper-pair formation.

In contrast to cuprates and conventional superconductors, the superconducting gap distribution in iron-based superconductors is rather diversified [3]. Nodeless isotropic gap distributions have been observed in $Ba_{1-x}K_xFe_2As_2$, $Ba_2Fe_{2-x}Co_xAs_2$, LiFeAs, $NaFe_{1-x}Co_xAs_2$, and $FeTe_{1-x}Se_x$ [3–9], whereas strong signatures of nodal superconducting gaps have been reported via the use of various experimental techniques in LaOFeP [10], LiFeP [11], underdoped $Ba_{1-x}K_xFe_2As_2$ [12,13], $BaFe_{2-x}Ru_xAs_2$ [14], KFe_2As_2 [15], FeSe [16], and $BaFe_2(As_{1-x}P_x)_2$ [3,12,14,17–21]. Similar nodal gap structures were expected for other nodal compounds, such as phosphorus-based iron pnictides [3]. Indeed, for the optimally doped compound $SrFe_2(As_{0.65}P_{0.35})_2$, evidence suggesting nodal superconductivity was obtained by performing phosphorus-31 nuclear magnetic resonance (^{31}P-NMR), specific-heat measurements, and London penetration depth measurements [22–24]. In this paper, we present our results from scanning tunneling microscopy and scanning tunneling spectroscopy (STM/STS) measurements on isovalently doped $SrFe_2(As_{1-x}P_x)_2$, confirming nodal superconductivity for the optimally doped ($x = 0.35$) and overdoped ($x = 0.46$) compound with a hint for $s_\pm$ pairing symmetry. While the undoped compounds have been investigated with STM [25,26], no STM/STS has been performed so far on doped samples suffering from a possible doping inhomogeneity. Here, STM provides a useful tool for investigation of the surface morphology and the superconducting gap by means of elastic tunneling. Inelastic tunneling is a precise tool that can be used to reveal the underlying bosonic structure in conventional superconductors [27,28]. We apply here inelastic tunneling to unconventional superconductors. Since for the optimally doped compound—$SrFe_2(As_{0.65}P_{0.35})_2$—the superconducting transition temperature T_c is about 30 K [29], it is unlikely that phonons are the particles responsible for the Cooper pairing [30,31]. Hence, the investigation of other excitations that could act as "pairing glue" is important. In particular, for the investigation of doped samples, STM is an appropriate method to address these samples due to its ability to spatially resolve the density of states (DOS). This allows us to directly determine the coherence length in the superconducting compounds from measurements of the local DOS as well.

Depending on the phosphorus concentration and temperature, $SrFe_2(As_{1-x}P_x)_2$ can be in the magnetic phase, the superconducting phase, or the normal conducting phase [29]. In the present paper, we investigated $SrFe_2(As_{1-x}P_x)_2$ by performing STS for four different doping concentrations. In the first part of the paper, we present the results of the optimally doped ($x = 0.35$) and overdoped ($x = 0.46$) superconducting compound. The method for measuring the superconducting gap and the coherence length will be explained therein. In the second part, possible inelastic excitations of these compounds are compared with those of the magnetic compound ($x = 0.2$) and the parent compound ($x = 0$).

II. METHODS AND RESULTS

The $SrFe_2(As_{1-x}P_x)_2$ single crystals were synthesized using the self-flux method [29]. For the superconducting compounds, T_c is about 30 K for the optimally doped and 18 K for the overdoped compound. All investigated crystals were cleaved at $p \sim 1 \times 10^{-10}$ mbar at 77 K, and afterward they were immediately transferred to the STM. Cleavage posts were glued onto the samples using a triple-axis manipulator (3D micrometer-drive lift from VIC International, Tokyo). Measurements were performed with a home-built Joule Thomson low-temperature STM (JT-STM) [32] at about 0.8 K. The JT-STM contains a magnet that enables entry into the Shubnikov phase of $SrFe_2(As_{1-x}P_x)_2$. Topographic

 ©2016 American Physical Society

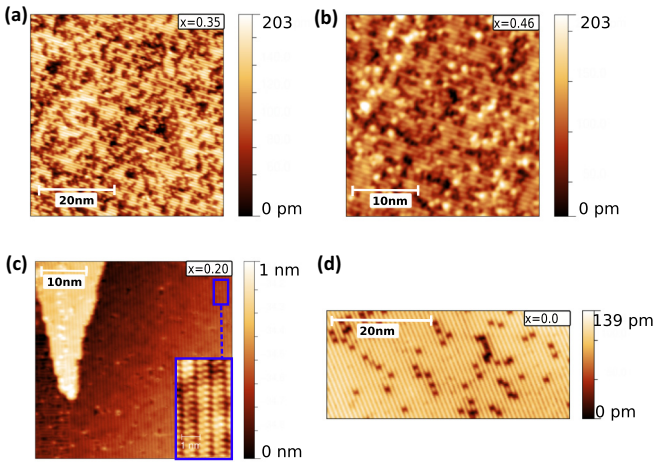

FIG. 1. Topographic images for (a) the optimally doped compound ($x = 0.35$) (50 nm × 50 nm^2, $U = 1$ V, $I = 100$ pA); (b) the overdoped compound ($x = 0.46$) (30 nm × 30 nm^2, $U = 7$ mV, $I = 1$ nA); (c) the underdoped compound ($x = 0.2$) (35 nm × 35 nm^2, $U = 80$ mV, $I = 1$ nA, and $U = 6.4$ mV, $I = 2$ nA for the inset); and (d) the parent compound with $x = 0$ (50 nm × 23 nm^2, $U = 600$ mV, $I = 1$ nA).

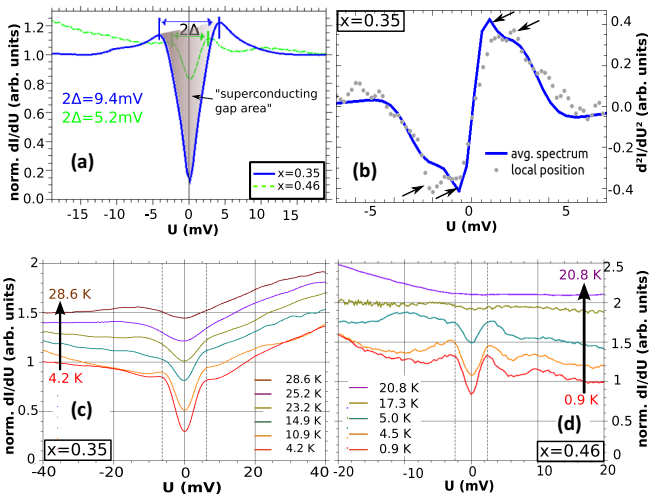

FIG. 2. (a) Spatially averaged superconducting gap over many spectra for the optimally doped (blue) and overdoped (dashed light-green) compound at $T = 0.8$ K ($I_{\rm set} = 2.15$ nA, $U_{\rm mod} = 1$ mV) (the shaded area displays the "superconducting gap area" as mentioned in the text), (b) numerical derivative of the optimally doped spectrum [from the curve in (a)] in blue and a spectrum of a local position in gray, (c) temperature dependence of the superconducting gap for the optimally doped compound ($x = 0.35$) ($I_{\rm set} = 5$ nA), and (d) temperature dependence of the superconducting gap for the overdoped compound ($x = 0.46$) ($I_{\rm set} = 3.5$ nA).

images for the four different compounds are shown in Fig. 1. Due to covalent bonds between Fe and As atoms, the FeAs layers are assumed to remain intact during the cleavage. In fact, the cleavage occurs either between the As and Sr layers or within the Sr layer, leaving half of the atoms of the Sr layer on the topmost layer forming a $(\sqrt{2} \times \sqrt{2})$ or (2×1) reconstruction [25,33].

In our measurements, a (2×1) reconstruction was present for all samples. However, the samples with higher doping concentrations ($x = 0.35$,0.46) showed more defects and impurities coming from the higher phosphorus concentration. The tunneling spectra [cf. Fig. 2(a)] are spatially averaged over many spectra. The width of the superconducting gap 2Δ was determined by the positions of the quasiparticle peaks, which occur at $\Delta = \pm 4.7$ mV for the optimally doped compound and $\Delta = \pm 2.6$ mV for the overdoped compound, as indicated in the figure. Even though they were measured at $T = 0.8$ K, the superconducting gap is V-shaped and does not go completely down to zero at zero bias. Nevertheless, the temperature dependence of the gap [see Figs. 2(c) and 2(d)] and the appearance of a vortex lattice by applying a magnetic field [see Figs. 4(a) and 4(c)] prove that the gap is indeed due to superconductivity. In Fig. 2(a), the superconducting gap of the optimally doped compound is compared to that of the overdoped compound.

Iron-based superconductors, as well as the present system, show a complicated Fermi surface characterized by five sets of Fermi sheets arising from the d-orbital of iron. Two of them form electronlike pockets at the M point, while the other three build up holelike pockets centered at the Γ point [33,34]. The different Fermi surfaces give rise to different gap values, characteristic of multiband superconductors. Indeed, our optimally doped sample shows a double-gap-like feature. This can be seen in Fig. 2(b), where we observe not only one dip-peak pair but also two features inside the V-shaped gap. The dip and peak features closest to zero bias correspond to the largest slope of the superconducting DOS shown in blue in Fig. 2(a). The peaks and dips, marked by arrows, correspond to local maxima of the slope of the superconducting DOS [blue line in Fig. 2(a)]. We exclude a site-dependent superconducting gap or doping inhomogeneities as the origin of the observed double-gap feature since it is even present in individual, local spectra. As an example, one of them is shown in gray in Fig. 2(b). Further hints for multiple gap values have been obtained experimentally in angular-resolved photoemission spectroscopy (ARPES) studies on Ba122-K40 [35] as well as in STM experiments on Ba122-Co6 [33,36].

The mentioned electron- and holelike Fermi surfaces are linked via scattering processes involving antiferromagnetic spin fluctuations [37]. In conjunction with this scattering process, if it was the mechanism of Cooper pair formation, an unconventional $s_\pm$ symmetry of the order parameter $\Psi_{\rm SC}$ was proposed [37] that exhibits different signs on the electron and hole pockets.

If the order parameter vanishes at some points on the Fermi surface, the quasiparticle density of states, which is averaged over all momenta, is thus not fully gapped anymore, and a V-shaped gap emerges. The results shown in Fig. 2 prove that the system $SrFe_2(As_{1-x}P_x)_2$ possesses a nodal superconducting gap, suggesting $s_\pm$-symmetry in this system. While the d-symmetry always induces a nodal gap due to symmetry in cuprates, in the pnictides the appearance of a V-shaped gap depends on the details of the compound under investigation. This effect was already observed experimentally in the comparison of tunneling spectra of $FeTe_{1-x}Se_x$, which are fully gapped [38], and FeSe, where a V-shaped gap was observed [16].

Next, we determined the coherence length of the optimally and overdoped compounds by using two different methods for both of them. On the one hand, we applied the power spectral density function (PSDF) on a measured superconducting gap map, and on the other hand, we applied a magnetic field to extract the coherence length from a vortex. First we describe the PSDF method.

A. PSDF method

Due to the random phosphorus doping, inhomogeneities within the sample lead to spatial variations of the superconducting order parameter on the minimal length scale set by the coherence length. Thinking about conventional superconductors, the superconducting ground state occurs due to a large number of overlapping Cooper-pair wave functions where the phase of the Cooper pair is the same as that of the superconducting ground state. In BCS theory, the coherence length ξ is related to the physical size of a single Cooper pair [39]. For $SrFe_2(As_{1-x}P_x)_2$, we assume that the spatial variation of doping concentration causing spatial variations of the pairing is convoluted with the wave function of the Cooper pairs. The size of a single Cooper pair can be estimated by using the probability distribution of a Cooper pair [40]. For our data analysis, we therefore use the Gaussian distribution

$$g(x,y) = \frac{1}{2\pi\sigma^2} e^{-\frac{x^2+y^2}{2\sigma^2}}. \quad (1)$$

In this case, we assume the coherence length to be the full width at half-maximum (FWHM) of (1),

$$\xi = \mathrm{FWHM} = 2\sigma\sqrt{2\ln(2)}. \quad (2)$$

To extract ξ, we performed spatially resolved STS measurements over an area of 30 nm $\times$ 30 nm^2 with 256 $\times$ 256 spectra. For each spectrum, the order parameter was evaluated. As the gap has a V shape, it is not sufficient to measure just the energy of the gap, i.e., the depth of the gap must also be considered. We thus numerically integrated the area of the V-shaped gap for each spectrum. Finally, a map of the superconducting gap area [as sketched in Fig. 2(a)] was generated [see Figs. 3(a) and 3(c)].

Such a map shows bright and dark areas. Bright areas correspond to large values for the superconducting gap area and hence to a pronounced superconducting behavior. In contrast, in the darker areas the superconductivity is suppressed. On these images, we applied the radial resolved PSDF, where the PSDF is the square of the absolute value of the Fourier transformation of a function [PSDF $= |\mathcal{F}(f(x,y))|^2$] [41,42]. We can calculate the coherence length assuming such an image consists of randomly distributed superconducting areas convoluted with a Gaussian distribution $g(x,y)$ representing the Cooper pairs with their coherence length,

$$|\mathcal{F}(\mathrm{image})|^2 = \underbrace{|\mathcal{F}(\mathrm{random})|^2}_{\mathrm{const}} * |\mathcal{F}(g(x,y))|^2. \quad (3)$$

Using the relationship (2), the coherence length can be extracted from $\mathcal{F}(g(x,y))$ as shown in Figs. 3(b) and 3(d). By averaging several measurements in different regions on the surface for the optimally doped compound as well as for the overdoped compound, we obtain for the in-plane superconducting coherence length a value of $\xi_{x=0.35} = 4.1 \pm 1.1$ nm for the optimally doped compound and $\xi_{x=0.46} = 2.3 \pm 0.8$ nm for the overdoped compound. To verify these results, we additionally determined the coherence length by using a second method, which we call the vortex method.

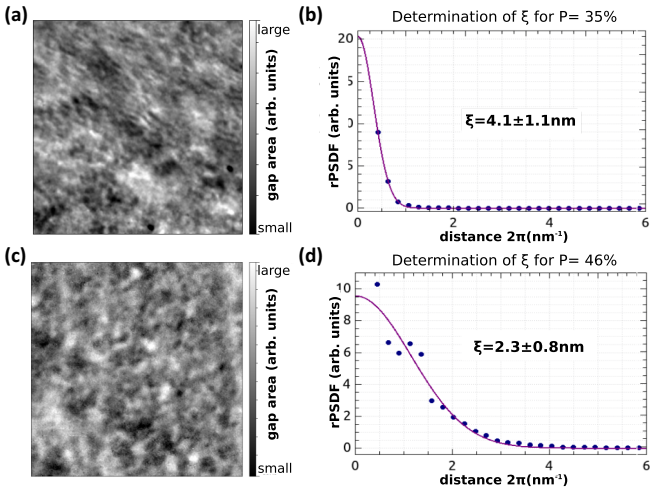

FIG. 3. (a) Spatially resolved map of the superconducting gap area for the optimally doped compound ($x = 0.35$) (30 $\times$ 30 nm^2, 256 $\times$ 256 pixel), (b) calculated radial resolved PSDF of the gap map shown in (a) (dots) and the applied fit shown as a solid line, (c) spatially resolved map of the superconducting gap area for the overdoped compound ($x = 0.46$) (35 $\times$ 35 nm^2, 256 $\times$ 256 pixel), and (d) calculated radial resolved PSDF of the gap map shown in (c) (dots) and the applied fit shown as a solid line.

B. Vortex method

By applying a magnetic field of 1 T, the optimally doped as well as the overdoped compound enter the Shubnikov phase. The vortex lattice could be resolved in d^2I/dU^2 maps. For this, we set the bias voltage to 2 and 1.2 mV, respectively, for the optimally doped and overdoped compound. These bias voltages correspond to the largest slope of the superconducting DOS in the optimally doped and the overdoped compound, visible as peaks in the second derivative of the tunneling current. Recording d^2I/dU^2 maps at this bias voltage allows us to distinguish superconducting and normal conducting areas. The superconducting areas appear brighter due to the pronounced gap around the Fermi energy. The vortex lattice is shown in Figs. 4(a) and 4(c).

In the vortex core, the material is in the normal state, where the superconducting order parameter $\Psi_{SC}(r) = |\Psi(r)|e^{i\theta}$ is completely suppressed. For an isolated vortex, the function $\Psi(r) = \Psi_\infty \tanh(\frac{r}{\sqrt{2}\xi})$ solves the Ginzburg-Landau equation, with r as the distance from the vortex core and Ψ_∞ as the value in the absence of a magnetic field [39,43]. By recording full STS spectra around the Fermi energy on points on a line through a vortex [see the lower right of Figs. 4(b) and 4(d)], it is possible to measure the spatial variation of the superconducting energy gap, i.e., $|\Psi(r)_{SC}| = |\Psi_\infty| \tanh(\frac{r}{\sqrt{2}\xi})$. The width of the superconducting energy gap can be determined by measuring the coherence peak separation. By fitting the

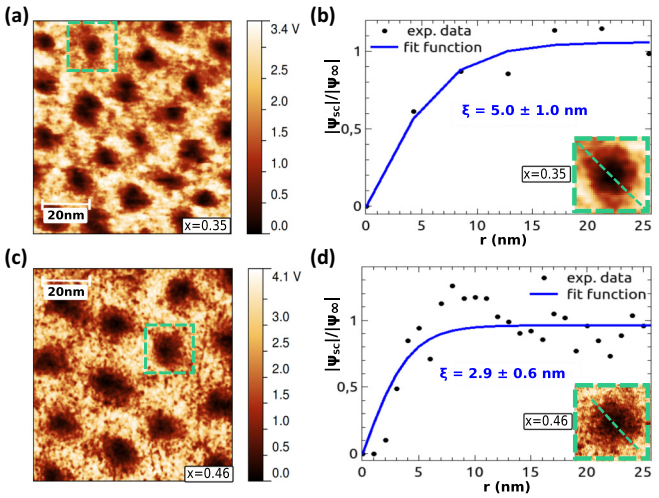

FIG. 4. (a) Vortex lattice of the optimally doped compound recorded as a d^2I/dU^2 map at $U = 2$ mV, and (b) measured normalized width of the superconducting energy gap obtained from individual tunneling spectra recorded along a line through a vortex that is marked with a green rectangle in (a) and (b) (dots). r represents the distance to the vortex core, where the superconducting order parameter is fully suppressed. The solid line represents the fit to the spatial dependence of the normalized width of superconducting energy gap. (c) Vortex lattice of the overdoped compound recorded as a d^2I/dU^2 map at $U = 1.2$ mV, and (d) analog to (b) for the overdoped compound.

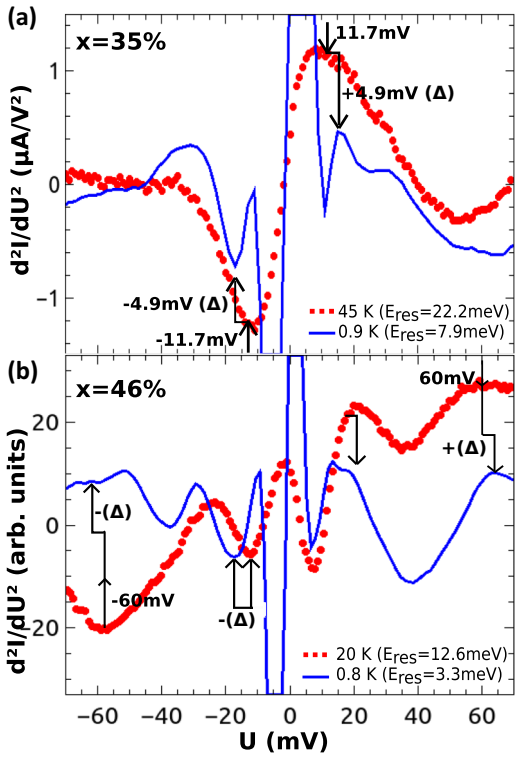

FIG. 5. (a) Optimally doped compound: d^2I/dU^2 spectrum for $T > T_c$ (red dots) and for $T < T_c$ (blue line) ($U_m = 4.3$ mV, $I_{set} = 21$ nA); (b) overdoped compound: d^2I/dU^2 spectrum for $T > T_c$ (red dots) ($U_m = 1.95$ mV, $I_{set} = 14$ nA) and for $T < T_c$ (blue line) ($U_m = 5$ mV, $I_{set} = 4.7$ nA).

measured width of the superconducting energy gap normalized to its value in the absence of a magnetic field $|\Psi(r)_{SC}|/|\Psi_\infty|$ with a function $f(r) = a\tanh(\frac{r}{\sqrt{2}\xi})$, the coherence length can be extracted.

The obtained data are plotted against the distance from the vortex, as shown in Figs. 4(b) and 4(d). As a result, we obtain $\xi = 5.0 \pm 1.0$ nm ($\xi = 2.9 \pm 0.6$ nm) for the optimally doped (overdoped) compound. The agreement with the PSDF method is rather good for the optimally as well as the overdoped compound. Nevertheless, the PSDF method is more accurate as it contains information on a higher number of local spectra. The vortex method requires us to measure along a line through the vortex, which should not move during the measurement. For the optimally doped compound in particular, the vortices were mobile even during scanning and were not well-pinned, as can also be seen in the vortex lattice in Fig. 4(a).

Finally, a theoretical estimation for the coherence length can be made by using the well-established relation $H_{c2} = \frac{\Delta_0}{2\pi\xi^2}$ [44]. For the optimally doped compound, the upper critical field H_{c2} is about 60 T [24]. This results in $\xi_{theo} \approx 2.34$ nm, which fits well with our results. Furthermore, if we compare these to values for the coherence length of similar systems, they are in the same order of magnitude [45].

III. INELASTIC TUNNELING SPECTROSCOPY

In a last step, we performed inelastic tunneling spectroscopy (ITS) for the four different doping concentrations. For the superconducting compounds ($x = 0.35/0.46$), ITS spectra were measured in the normal conducting state ($T > T_c$) and the superconducting state ($T < T_c$), respectively. In Fig. 5(a), spectra for the optimally doped compound are shown. In the normal conducting state (red line), a dip-peak pair at 11.7 mV is visible, which could be assigned to an optical phonon mainly arising from the atomic displacements of As and Fe atoms [46,47]. Furthermore, this peak exists in the superconducting state as well (blue line), where it is shifted by about 4.9 mV away from the Fermi energy due to the existence of the SC gap of $\Delta = 4.7$ mV. The results of the same measurement for the overdoped compound are shown in Fig. 5(b). In this case, a peak around 16.3 mV is visible in the normal state (red line), which could either be referred to the same phonon as in Fig. 5(a) or to another optical phonon in this system related to atomic displacements of the Sr atoms [46]. For the superconducting state, these features are shifted by about 2.3 mV away from the Fermi energy again due to the existing superconducting gap, which is 2.6 mV in the case of the overdoped compound. Furthermore, for the overdoped compound [see Fig. 5(b)], an additional peak is visible at 60 mV for the superconducting as well as for the normal state, even though the peak in the superconducting state is quite weak at negative bias site. Since the Van-Hove singularities in the phonon-dispersion relation occur only in an energy range of 13–40 meV for the parent compound [46,48], this peak cannot be assigned to any phonon. A possible explanation for this peak would be a magnon within this energy. Using optical techniques, excitations at 68 meV have been found in the parent compound and have been assigned to magnons [49].

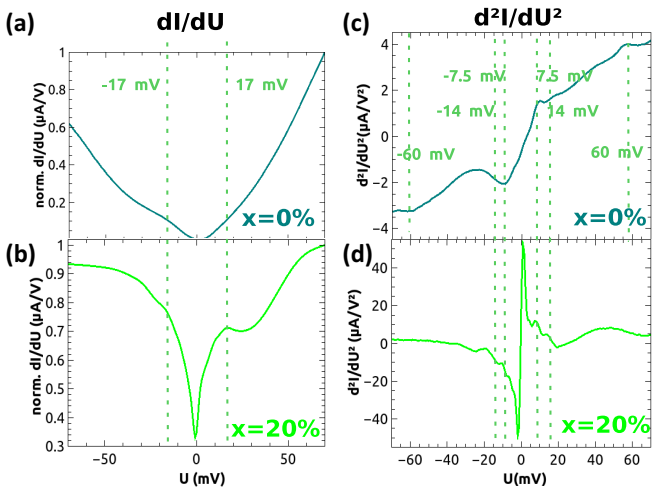

FIG. 6. (a) Parent compound: 100 averaged dI/dU spectra over an area of 20×20 nm^2 at $T = 0.8$ K ($U_m = 2.9$ mV), (b) magnetic compound with $x = 0.2$: 90 averaged dI/dU spectra over an area of 1.6×1.6 nm^2 at $T = 0.8$ K ($U_m = 761$ μV), (c) corresponding d^2I/dU^2 measurement of (a), and (d) corresponding d^2I/dU^2 measurement of (b).

The difference of 8 meV compared to our measurements could be explained due to the phosphorus concentration in our overdoped compound or the energy resolution of only about 9 meV for the spectra above T_c. Hence, we suggest that the observed dip-peak at 60 meV in the overdoped compound is due to a magnon.

Similar measurements were done for the magnetic compounds ($x = 0/0.2$). Conductance measurements are shown in Figs. 6(a) and 6(b), whereas measurements of inelastic excitations are shown in Figs. 6(c) and 6(d). For the parent compound, the averaged dI/dU spectrum in Fig. 6(a) shows a V-shaped gap of $2\Delta \approx 34$ meV around the Fermi energy. Even though the gap is rather broad, from the separation between the two edges in the normalized spectra we can estimate weak shoulders appearing at $\Delta \approx \pm 17$ meV. We suggest that this gap represents a spin gap due to nested electron bands causing a spin density wave [50]. The same gap can be seen much clearer in the underdoped compound, as shown in Fig. 6(b).

In Figs. 6(c) and 6(d), features of the spin gap and several inelastic excitations are visible either as clear peaks in the spectra or weak shoulders. At ± 7.5 mV, both compounds show a dip-peak pair that corresponds to the largest slope of the spin gap shown in Figs. 6(a) and 6(b). Furthermore, both samples show a feature at ± 14 mV, i.e., at similar energies to the excitations observed in the superconducting samples. We attribute these features to phonons [46,47]. Finally, we have observed broad features around 60 mV in the parent compound. These energies are similar to the broad features found in the overdoped sample, suggesting a magnetic origin as well. Thus, we recall some of the excitations observed in the superconducting samples and in the magnetic samples linking the two phases.

IV. CONCLUSION

In summary, we revealed a nodal superconducting gap for the optimally doped and overdoped compound of $SrFe_2(As_{1-x}P_x)_2$ indicating an $s_\pm$ symmetry in this system. Furthermore, we determined the superconducting coherence length for the respective compounds of the order of a few nm. While this is significantly smaller than the values found in conventional superconductors, it is of the same order of magnitude compared to other pnictide superconductors. Due to the small coherence length, the local stoichiometry affects the superconducting properties [51]. Thus, for optimizing the superconductive properties, the doping needs to be homogeneous on the short length scales of the coherence length. The spectroscopic measurements indicate electron-phonon coupling in all four compounds. In addition to phonons, we could identify magnetic excitations in the inelastic spectra, giving further evidence for magnon-driven superconductivity.

ACKNOWLEDGMENTS

The authors acknowledge funding by the DFG under project WU 349/12-1, and fruitful discussions with Jörg Schmalian and Patrik Hlobil.

[1] Y. Kamihara, T. Watanabe, M. Hirano *et al.*, J. Am. Chem. Soc. **130**, 3296 (2008).

[2] P. Dai, H. Luo, and M. Wang, in *Iron-Based Superconductivity*, Springer Series in Materials Science (Springer, Berlin, 2015), Chap. 5.

[3] Y. Zhang, Z. R. Ye, and D. L. Feng, in *Iron-Based Superconductivity*, Springer Series in Materials Science (Springer, Berlin, 2015), Chap. 4.

[4] H. Ding, P. Richard, K. Nakayama, K. Sugawara, T. Arakane, Y. Sekiba, A. Takayama, S. Souma, T. Sato, T. Takahashi, Z. Wang, X. Dai, Z. Fang, G. F. Chen, J. L. Luo, and N. L. Wang, Europhys. Lett. **83**, 47001 (2008).

[5] K. Terashima, Y. Sekiba, J. H. Bowen, K. Nakayama, T. Kawahara, T. Sato, P. Richard, Y.-M. Xu, L. J. Li, G. H. Cao, Z.-A. Xu, H. Ding, and T. Takahashi, Proc. Natl. Acad. Sci. USA **106**, 7330 (2009).

[6] H. Miao, P. Richard, Y. Tanaka, K. Nakayama, T. Qian, K. Umezawa, T. Sato, Y.-M. Xu, Y.-B. Shi, N. Xu, X.-P. Wang, P. Zhang, H.-B. Yang, Z.-J. Xu, J. S. Wen, G.-D. Gu, X. Dai, J.-P. Hu, T. Takahashi, and H. Ding, Phys. Rev. B **85**, 094506 (2012).

[7] Z.-H. Liu, P. Richard, K. Nakayama, G.-F. Chen, S. Dong, J.-B. He, D.-M. Wang, T.-L. Xia, K. Umezawa, T. Kawahara, S. Souma, T. Sato, T. Takahashi, T. Qian, Y. Huang, N. Xu, Y. Shi, H. Ding, and S.-C. Wang, Phys. Rev. B **84**, 064519 (2011).

[8] K. Umezawa, Y. Li, H. Miao, K. Nakayama, Z. H. Liu, P. Richard, T. Sato, J. B. He, D. M. Wang, G. F. Chen, H. Ding, T. Takahashi, and S. C. Wang, Phys. Rev. Lett. **108**, 037002 (2012).

[9] S. V. Borisenko, V. B. Zabolotnyy, A. A. Kordyuk, D. V. Evtushinsky, T. K. Kim, I. V. Morozov, R. Follath, and B. Buchner, Symmetry **4**, 251 (2012).

[10] J. D. Fletcher, A. Serafin, L. Malone, J. G. Analytis, J. H. Chu, A. S. Erickson, I. R. Fisher, and A. Carrington, Phys. Rev. Lett. **102**, 147001 (2009).

[11] K. Hashimoto, S. Kasahara, R. Katsumata, Y. Mizukami, M. Yamashita, H. Ikeda, T. Terashima, A. Carrington, Y. Matsuda, and T. Shibauchi, Phys. Rev. Lett. **108**, 047003 (2012).

[12] Y. Zhang, Z. R. Ye, Q. Q. Ge, F. Chen, J. Jiang, M. Xu, B. P. Xie, and D. L. Feng, Nat. Phys. **8**, 371 (2012).

[13] J.-Ph. Reid, M. A. Tanatar, X. G. Luo, H. Shakeripour, S. René de Cotret, N. Doiron-Leyraud, J. Chang, B. Shen, H.-H. Wen, H. Kim, R. Prozorov, and L. Taillefer, arXiv:1105.2232.

[14] X. Qiu, S. Y. Zhou, H. Zhang, B. Y. Pan, X. C. Hong, Y. F. Dai, M. J. Eom, J. S. Kim, Z. R. Ye, Y. Zhang, D. L. Feng, and S. Y. Li, Phys. Rev. X **2**, 011010 (2012).

[15] J. K. Dong, S. Y. Zhou, T. Y. Guan, H. Zhang, Y. F. Dai, X. Qiu, X. F. Wang, Y. He, X. H. Chen, and S. Y. Li, Phys. Rev. Lett. **104**, 087005 (2010).

[16] C.-L. Song, Y.-L. Wang, P. Cheng, Y.-P. Jiang, W. Li, T. Zhang, Z. Li, K. He, L. Wang, J.-F. Jia, H.-H. Hung, C. Wu, X. Ma, X. Chen, and Q.-K. Xue, Science **332**, 1410 (2011).

[17] K. Hashimoto, M. Yamashita, S. Kasahara, Y. Senshu, N. Nakata, S. Tonegawa, K. Ikada, A. Serafin, A. Carrington, T. Terashima, H. Ikeda, T. Shibauchi, and Y. Matsuda, Phys. Rev. B **81**, 220501 (2010).

[18] Y. Nakai, T. Iye, S. Kitagawa, K. Ishida, S. Kasahara, T. Shibauchi, Y. Matsuda, and T. Terashima, Phys. Rev. B **81**, 020503(R) (2010).

[19] J. S. Kim, P. J. Hirschfeld, G. R. Stewart, S. Kasahara, T. Shibauchi, T. Terashima, and Y. Matsuda, Phys. Rev. B **81**, 214507 (2010).

[20] Y. Wang, J. S. Kim, G. R. Stewart, P. J. Hirschfeld, S. Graser, S. Kasahara, T. Terashima, Y. Matsuda, T. Shibauchi, and I. Vekhter, Phys. Rev. B **84**, 184524 (2011).

[21] M. Yamashita, Y. Senshu, T. Shibauchi, S. Kasahara, K. Hashimoto, D. Watanabe, H. Ikeda, T. Terashima, I. Vekhter, A. B. Vorontsov, and Y. Matsuda, Phys. Rev. B **84**, 060507(R) (2011).

[22] T. Dulguun, H. Mukuda, T. Kobayashi, F. Engetsu, H. Kinouchi, M. Yashima, Y. Kitaoka, S. Miyasaka, and S. Tajima, Phys. Rev. B **85**, 144515 (2012).

[23] J. Murphy, C. P. Strehlow, K. Cho, M. A. Tanatar, N. Salovich, R. W. Giannetta, T. Kobayashi, S. Miyasaka, S. Tajima, and R. Prozorov, Phys. Rev. B **87**, 140505(R) (2013).

[24] H. Takahashi, T. Okada, Y. Imai, K. Kitagawa, K. Matsubayashi, Y. Uwatoko, and A. Maeda, Phys. Rev. B **86**, 144525 (2012).

[25] M. Dreyer, M. Gubrud, S. Saha, N. P. Butch, K. Kirshenbaum, and J. Paglione, J. Phys.: Condens. Matter **23**, 265702 (2011).

[26] A. Dutta, N. Kumar, A. Thamizhavel, and A. K. Gupta, Phys. Status Solidi B **253**, 340 (2016).

[27] M. Schackert, T. Märkl, J. Jandke, M. Hölzer, S. Ostanin, E. K. U. Gross, A. Ernst, and W. Wulfhekel, Phys. Rev. Lett. **114**, 047002 (2015).

[28] J. Jandke, P. Hlobil, M. Schackert, W. Wulfhekel, and Jörg Schmalian, Phys. Rev. B **93**, 060505 (2016).

[29] T. Kobayashi, S. Miyasaka, and S. Tajima, J. Phys. Soc Jpn. **81**, SB045 (2012).

[30] W. L. McMillan, Phys. Rev. **167**, 331 (1968).

[31] L. Stojchevska, P. Kusar, T. Mertelj, V. V. Kabanov, X. Lin, G. H. Cao, Z. A. Xu, and D. Mihailovic, Phys. Rev. B **82**, 012505 (2010).

[32] L. Zhang, T. Miyamachi, T. Tomani, R. Dehm, and W. Wulfhekel, Rev. Sci. Instrum. **82**, 103702 (2011).

[33] J. E. Hoffman, Rep. Prog. Phys. **74**, 124513 (2011).

[34] H.-H. Wen and S. Li, Annu. Rev. Condens. Matter Phys. **2**, 121 (2011).

[35] T. Shimojima, F. Sakaguchi, K. Ishizaka, Y. Ishida, T. Kiss, M. Okawa, T. Togashi, C.-T. Chen, S. Watanabe, M. Arita, K. Shimada, H. Namatame, M. Taniguchi, K. Ohgushi, S. Kasahara, T. Terashima, T. Shibauchi, Y. Matsuda, A. Chainani, and S. Shin, Science **332**, 564 (2011).

[36] M. L. Teague, G. K. Drayna, G. P. Lockhart, P. Cheng, B. Shen, H.-H. Wen, and N.-C. Yeh, Phys. Rev. Lett. **106**, 087004 (2011).

[37] I. I. Mazin, D. J. Singh, M. D. Johannes, and M. H. Du, Phys. Rev. Lett. **101**, 057003 (2008).

[38] T. Hanaguri, S. Niitaka, K. Kuroki, and H. Takagi, Science **328**, 474 (2010).

[39] J. F. Annett, *Superconductivity, Superfluids and Condensates* (Oxford University Press, Oxford, 2004), p. 77.

[40] A. Marouchkine, *Room-Temperature Superconductivity* (Cambridge International Science Publishing, Cambridge, 2004).

[41] J. J. Lee, D. Garinis, D. L. Frost, J. H. S. Lee, and R. Knystautas, Shock Waves **5**, 169 (1995).

[42] P. Hertel, *Theoretische Physik* (Springer-Lehrbuch, Berlin, 2007), Kap. 8, p. 356.

[43] C. P. Poole, H. A. Farach, and R. J. Creswick, *Superconductivity* (Academic Press, Amsterdam, 1995).

[44] W. Buckel and R. Kleiner, *Supraleitung, Grundlagen und Anwendung*, 6th ed. (Wiley-Verlag, Weinheim, 2004).

[45] C. J. van der Beek, M. Konczykowski, S. Kasahara, T. Terashima, R. Okazaki, T. Shibauchi, and Y. Matsuda, Phys. Rev. Lett. **105**, 267002 (2010).

[46] A. P. Litvinchuk, V. G. Hadjiev, M. N. Iliev, B. Lv, A. M. Guloy, and C. W. Chu, Phys. Rev. B **78**, 060503(R) (2008).

[47] H. Kobayashi, S. Ikeda, Y. Yoda, H. Nakamura, and M. Machida, Phys. Rev. B **84**, 184304 (2011).

[48] M. Zbiri, R. Mittal, S. Rols, Y. Su, Y. Xiao, H. Schober, S. L. Chaplot, M. R. Johnson, T. Chatterji, Y. Inoue, S. Matsuishi, H. Hosono, and T. Brueckel, J. Phys.: Condens. Matter **22**, 315701 (2010).

[49] J. N. Hancock, S. I. Mirzaei, J. Gillett, S. E. Sebastian, J. Teyssier, R. Viennois, E. Giannini, and D. van der Marel, Phys. Rev. B **82**, 014523 (2010).

[50] D. Hsieh, Y. Xia, L. Wray, D. Qian, K. Gomes, A. Yazsani, G. F. Chen, J. L. Luo, N. L. Wang, and M. Z. Hasan, arXiv:0812.2289 (cond-mat.supr-con).

[51] A. Malozemoff, J. Mannhart, and D. Scalapino, Phys. Uns. Zeit **37**, 162 (2006).